Supporting Information

# Conjugated crosslinks boost the conductivity and stability of a single crystalline metal-organic framework

Hua-Qun Zhou,‡[a] Yonghe He,‡[a] Jie-Ying Hu,[a] Lai-Hon Chung,[a] Qinfen Gu,[b] Wei-Ming Liao,*[a] Matthias Zeller,[c] Zhengtao Xu,*[d] and Jun He*[a]

[a] School of Chemical Engineering and Light Industry, Guangdong University of Technology, Guangzhou 510006, Guangdong, China

[b] Australian Synchrotron, Australian Nuclear Science and Technology Organization, 800 Blackburn Road, Clayton, Victoria, Australia

[c] Department of Chemistry, 560 Oval Drive, Purdue University, West Lafayette, Indiana, 47907, United States.

[d] Department of Chemistry, City University of Hong Kong, 83 Tat Chee Avenue, Kowloon, Hong Kong, China

* Corresponding author.

*E-mail: wmliao@gdut.edu.cn, junhe@gdut.edu.cn, zhengtao@cityu.edu.hk*

‡ These authors contributed equally to this work.

## Table of Contents

## Experimental details

**General procedure.** Starting materials, reagents, and solvents were purchased from commercial sources (J&K, Aldrich and Acros) and used without further purification. Elemental analysis (EA) was performed with a Vario Micro CUBE CHN elemental analyzer. FT-IR spectra were obtained using a Nicolet Avatar 360 spectrophotometer. Nuclear magnetic resonance (NMR) spectra were recorded at 298 K on a 400 MHz Bruker superconducting magnet high-field NMR spectrometer, with working frequencies of 400 MHz for $^{1}$H, 376 MHz for $^{19}$F and 100 MHz for $^{13}$C nuclei. Chemical shifts are reported in ppm relative to the signals corresponding to the residual non-deuterated solvents, with tetramethylsilane (TMS) as the internal standard. Thermogravimetric analyses (TG) were carried out in a nitrogen stream using PerkinElmer Thermal analysis equipment (STA 6000) with a heating rate of 10 °C/min. Powder X-ray diffraction data were collected in reflection mode at room temperature on a Rigaku Smart Lab diffractometer with mixture of Cu-Kα1 (λ = 1.54056 Å) and Cu-Kα2 (λ = 1.5418 Å) radiation. The X-ray tube operated at a voltage of 30 kV and a current of 30 mA. Scanning electron microscopy (SEM) images were obtained from a field-emission scanning electron microscope (Hitachi, SU8220).

**Single crystal X-ray crystallography.**

Single crystal data for **$CH_3$BPD-4F4TS** were collected using a Bruker APEX-II CCD diffractometer with an I-mu-S micro-focus X-ray source using Cu Kα radiation (λ = 1.54178). Data were collected at 300 K. Data were collected, reflections were indexed and processed, and the files scaled and corrected for absorption using APEX3 v2018. The space group was assigned and the structure was solved by direct methods using XPREP within the SHELXTL suite of programs[1] and refined by full matrix least squares against $F^2$ with all reflections using Shelxl2018[2] using the graphical interface Shelxle[3]. C-H bond distances were constrained to 0.95 Å for

aromatic C-H and to 0.98 Å for $CH_3$ moieties, respectively. Methyl $CH_3$ were allowed to rotate but not to tip to best fit the experimental electron density. $U_{iso}$(H) values were set to a multiple of $U_{eq}$(C) with 1.5 for $CH_3$ and 1.2 for C-H, respectively. The four thiophene rings were refined as disordered by approximate 180° rotations. All thiophene moieties were restrained to have similar geometries (SAME command of Shelxl). $U^{ij}$ components of ADPs for disordered atoms closer to each other than 2.0 Angstrom were restrained to be similar. Subject to these conditions the occupancy ratios refined to 0.406(5) to 0.594(5) (ring of S2), to to 0.790(5) to 0.210(5) (ring of S4), to 0.536(5) to 0.464(5) (ring of S6), to 0.890(4) to 0.110(4) (ring of S8). Additional details are given in Table S1. Complete crystallographic data for **$CH_3$BPD-4F4TS**, in CIF format, have been deposited with the Cambridge Crystallographic Data Centre as CCDC 2026236. These data can be obtained free of charge from The Cambridge Crystallographic Data Centre via www.ccdc.cam.ac.uk/data_request/cif.

Single crystal X-ray diffraction (SCXRD) data for **ZrBPD-4F4TS** and **ZrBPD-4F4TS-Ox** were collected on MX2 beamline diffractometer, Australian Synchrotron, ANSTO. X-rays of wavelength $\lambda$ = 0.70926 Å were created using a finely-focused in-vacuum undulator equipped with a microcollimator. Beam size at the sample was 25 x 15 μm. Data were collected using a Dectris EIGER 16M detector. The crystal was kept at 100 K during data collection. Each crystal SCXRD data was collected with 360 degrees (0.1 degree rotation step), in total 3600 images. Data were processed using XDS. The space groups were assigned and the structure was solved by direct methods using XPREP within the SHELXTL suite of programs and refined by full matrix least squares against $F^2$ with all reflections using Shelxl2018 using the graphical interface Shelxle. Real and imaginary dispersion terms for the used wavelength were applied[4].

Full and unambiguous modeling of the two structures proved difficult due to intrinsic disorder of large parts of the structure. Connecting ligands are known from elemental analysis and other techniques to be partially absent and replaced by other

terminal donor entities (tentatively assigned as formic acid for a formula of $Zr_6O_4(OH)_4(C_{30}H_{12}F_4O_4S_8)_{3.8}(HCOO)_{4.4}(H_2O)_6$). Disorder between 4F4TS and formic acid is not resolved in the XRD data for **ZrBPD-4F4TS** and **ZrBPD-4F4TS-Ox** and was ignored in model building (refinement of occupancies is not possible due to large extinction effects caused by the low mosaicity of the crystals paired with the high beam line X-ray intensity. Extinction effects affect mostly the not disordered heavy Zr atoms, making refinement of occupancy ratios between Zr and ligands unreliable). Oxo and hydroxo groups of the Zr-cluster are 1:1 disordered. Connecting ligands were thus refined as fully occupied. Ligands are systematically disordered by crystal symmetry, with two equally occupied orientations present for all atoms other than the carboxylate groups. The thiophenethiol moieties are ill defined, with large thermal libration paired with unresolved disorder. They were refined as not disordered, using strict geometry restraints equivalent to a rigid body refinement. Thiophenethiol moieties overlap with their symmetry equivalent counterparts from neighboring ligands, with every thiophenethiol moiety being mutually incompatible with five of its symmetry equivalent counterparts, thus limiting the occupancy of each thiophenethiol moiety to one sixth (ignoring unresolved disorder), in tentative agreement with the occupancy ratio found by elemental analysis for **ZrBPD-4F4TS**. Differences between **ZrBPD-4F4TS** and **ZrBPD-4F4TS-Ox** are not resolved and the same structural model has been applied to both.

**Synthesis of dimethyl 2,2',5,5'-tetrafluoro-3,3',6,6'-tetrakis(thiophenethiol) -[1,1'-biphenyl]-4,4'-dicarboxylate ($CH_3$BPD-4F4TS).** 2,2',3,3',5,5',6,6'-octafluoro-[1,1'-biphenyl]-4,4'-dicarboxylate (OFBPD) (2.06 g, 4.97 mmol) and potassium carbonate (3.74 g, 27.1 mmol) were charged into a 100 mL flask, followed by the addition of 26 mL dry DMF. Then a mixture of 2 mL 2-thiophenethiol and 4 mL DMF was injected. The flask was capped and the mixture was stirred at room temperature for 2 h. The obtained mixture was poured into

water (50 mL) and extracted with ethyl acetate (3 × 30 mL). The combined organic layer was then washed with water (3 × 50 mL) and dried with anhydrous $MgSO_4$. Crude product was obtained after the removal of organic solvent using a rotary evaporator. Further purification by column chromatography (silica gel, with PE and EA as the eluent) afforded a pink solid ($CH_3$BPD-4F4TS, 2.7 g, yield 68 % based on OFBPD). $^1$H NMR (600 MHz, $CDCl_3$) δ = 7.37 (dd, *J* = 5.8, 0.6, 2H), 7.28 (d, *J* = 3.4, 2H), 7.22 (dd, *J* = 5.3, 1.1, 2H), 6.95 (dd, *J* = 5.3, 3.6, 2H), 6.84 (d, *J* = 3.0, 2H), 6.80 (dd, *J* = 5.3, 3.7, 2H), 4.01 (s, 6H). $^{19}$F NMR (376 MHz, $CDCl_3$) δ = -105.10 (d, *J* = 15.5), -110.38 (d, *J* = 15.6). $^{13}$C NMR (150 MHz, $CDCl_3$) δ = 163.37 (d, *J* = 1.9), 156.14 (dd, *J*= 110.1, 2.8), 154.48 (dd, *J* = 111.4, 2.9), 136.13 (s), 135.63 (s), 131.26 (s), 131.20 (s), 130.02 (s), 129.14 (s), 127.97 (d, *J* = 22.2), 127.74 (d, *J* = 19.4), 127.68 (s), 127.62 (s), 126.19 (d, *J* = 20.4), 123.62 (dd, *J* = 23.0, 3.0), 53.48 (s). FT-IR (KBr pellet, ν/cm$^{-1}$): 3458 (w), 3100 (w), 3080 (w), 2956 (w), 2946 (w), 1738 (s), 1590 (w), 1436 (s), 1396 (s), 1335 (w), 1297 (s), 1250 (s), 1212 (s), 1148 (s), 1089 (w), 1068 (w), 1053 (w), 1009 (m), 985 (m), 954 (m),918 (w), 886 (m), 842 (s), 808 (w), 789 (w), 753 (w), 717 (s), 692 (s), 618 (w).

**Synthesis of 2,2',5,5'-tetrafluoro-3,3',6,6'-tetrakis(thiophenethiol)-[1,1'-biphenyl] -4,4'-dicarboxylic acid ($H_2$BPD-4F4TS).** A two-neck round-bottomed flask (100 mL) was loaded with a magnetic stirring bar and powder of $CH_3$BPD-4F4TS (2.04 g, 2.56 mmol), followed by repetition of evacuation and refilling with $N_2$ thrice. A solution of NaOH (2.4 g, 60 mmol) in EtOH (20 mL) and $H_2O$ (10 mL) was degassed and injected into the flask *via* cannula under an $N_2$ stream. The flask was then connected to a condenser and the mixture was refluxed for 3 h under $N_2$ protection. The resultant mixture was subsequently cooled to room temperature and poured slowly into water (50 mL) and HCl (10%) with vigorous stirring. The pH value was then kept to be lower than 2 for complete precipitation. The product was collected by suction filtration, washed with water and dried for solvothermal synthesis without further purification.

Yield: 1.88 g (95.4%, based on $CH_3$BPD-4F4TS). $^1$H NMR (400 MHz, DMSO) δ = 7.75 (d, *J* = 5.3, 2H), 7.59 (d, *J* = 5.1, 2H), 7.34 (d, *J* = 3.4, 2H), 7.10 – 7.05 (m, 2H), 6.93 – 6.89 (m, 2H), 6.88 (d, *J* = 3.2, 2H).$^{19}$F NMR (376 MHz, DMSO) δ = -105.89 (d, *J* = 15.8, 1H), -111.75 (d, *J* = 16.1, 1H). $^{13}$C NMR (150 MHz, DMSO) δ = 163.16 (s), 155.11 (d, *J* = 224.0), 153.45 (dd, *J* = 223.3, 2.5), 129.91 (d, *J* = 23.7), 128.53 (s), 128.08 (s), 127.99 (s), 127.82 (s), 126.72 (d, *J* = 20.5), 124.61 (d, *J* = 20.3), 122.60 (dd, *J* = 22.6, 4.1). FT-IR (KBr pellet, ν/cm$^{-1}$): 3445 (w), 3089 (m), 2956 (m), 2920 (m), 2852 (m), 2616 (m), 2516 (m), 1712 (s), 1588 (w), 1536 (w), 1431 (m), 1397 (s), 1293 (m), 1253 (s), 1217 (s), 1167 (w), 1084 (w), 1053 (w), 987 (w), 894 (m), 841 (s), 811 (m), 703 (s), 663 (w), 640 (w), 612 (w), 570 (w).

## MOF syntheses, characterizations and measurements

**Self-assembly synthesis of ZrBPD-4F4TS.** To a 25-mL Schlenk tube, $ZrCl_4$ (450 mg, 1.93 mmol), $H_2$BPD-4F4TS (720 mg, 0.94 mmol), trifluoroacetic acid (276 mg, 2.42 mmol) and DMF (18 mL) were added. The mixture was sonicated for 5 min to form a well-dispersed suspension. Then the tube was sealed with a Teflon cap and heated at 120 °C in an oven for 72 h, followed by natural cooling to room temperature, during which colorless octahedron-shaped single crystals were formed. The freshly prepared crystals were immersed in DMF (4 mL) thrice, and each time the crystals were soaked for 6 hours at 80 °C before the DMF was decanted (144 mg, 15% based on $H_2$BPD-4F4TS). Elemental analysis found [C (36.22%), H (1.56%), S (25.09%), N (0%)], a fitting formula can be determined to be $Zr_6O_4(OH)_4(C_{30}H_{12}F_4O_4S_8)_{3.8}(HCOO)_{4.4}(H_2O)_6$ (m.w. 3907), which gives a calculated profile as [C (36.39%), H (1.70%), S (24.95%), N (0%)].

**Activation of ZrBPD-4F4TS.** A thimble (e.g., made from folding filter paper) containing as-made sample of ZrBPD-4F4TS crystals (100 mg) was loaded into the main chamber of a Soxhlet extractor. The Soxhlet extractor was connected to a

250-mL round-bottomed flask including acetone (150 mL) and a magnetic stirring bar, and then equipped with a water condenser. The flask was heated to 100 °C with an oil bath for 3 days. The filter paper was then taken out and the solid was heated at 120 °C under vacuum to give the activated ZrBPD-4F4TS sample.

**Preparation of ZrBPD-4F4TS-Ox.** To a 25-mL Schlenk tube, activated ZrBPD-4F4TS (100 mg, 0.026 mmol), $FeCl_3$ (400 mg, 2.47 mmol), nitromethane (15 mL) and toluene (5 mL) were added. The mixture was sonicated for 5 min to form a well-dispersed solution. Then the tube was sealed with a Teflon cap and heated at 90 °C in an oven for 120 h, followed by natural cooling to room temperature, during which a brown powder was formed. The brown powder was washed with nitromethane, methanol and acetone several times and then dried in air to afford the as-made ZrBPD-4F4TS-Ox.

**Activation of ZrBPD-4F4TS-Ox.** A thimble (e.g., made from folding filter paper) containing an as-made sample of ZrBPD-4F4TS-Ox crystals (100 mg) was loaded into the main chamber of a Soxhlet extractor. The Soxhlet extractor was connected to a 250-mL round-bottom including methanol (150 mL) and a magnetic stirring bar, and then equipped with a water condenser. The flask was heated to 100 °C with an oil bath for 3 days. The filter paper was then taken out and the solid was heated at 120 °C under vacuum to give the activated ZrBPD-4F4TS-Ox sample.

**Treatment by HF and HCl solution of ZrBPD-4F4TS and ZrBPD-4F4TS-Ox.** About 15 mg of as-made ZrBPD-4F4TS (or ZrBPD-4F4TS-Ox) (containing about 2.1 mg, 0.023 mmol Zr) was placed into a 5-mL glass bottle, followed by addition of 2 mL dimethyl sulfoxide, 40 µL (48 mg solution, 0.48 mmol of HCl) or 120 µL (144 mg solution, 1.44 mmol of HCl) of hydrochloric acid (36% by weight, density 1.2 g/mL) and 10 mg of sodium fluoride (equivalent to 4.8 mg, 0.24 mmol of HF in about 2.3 gram of solution, i.e., 0.2% for HF, and 0.36% or 1.8% for HCl by weight). After heating in an oil bath at

85 °C for 30 min, ZrBPD-4F4TS was completely dissolved while ZrBPD-4F4TS-Ox was not (see Fig. S14). The centrifuged supernatants were used for $^{1}H$ and $^{19}F$ NMR measurements.

**Solution polymerization of Preparation of $H_2$BPD-4F4TS to form $H_2$BPD-4F4TS-*p*.** To a 25-mL Schlenk tube, $H_2$BPD-4F4TS (50 mg, 0.065 mmol), $FeCl_3$ (126 mg, 0.78 mmol) and anhydrous dichloromethane (5 mL) were added. The mixture was sonicated for 5 min to form a solution. Then the tube was sealed with a Teflon cap and the mixture was stirred at 60 °C in oil bath for 2 h, during which a yellow solid was formed. After cooling to room temperature, the insoluble yellow solid was collected by suction filtration, washed with methanol (5 × 10 mL), dichloromethane (5 × 10 mL) and acetone (3 × 10 mL) and then dried in air to afford the $H_2$BPD-4F4TS-*p* polymer product. Yield: 39 mg (78.4%, based on $H_2$BPD-4F4TS). FT-IR (KBr pellet, ν/cm$^{-1}$): 3445 (w), 3089 (m), 2956 (m), 2920 (m), 2852 (m), 2565 (m), 1712 (s), 1588 (w), 1536 (w), 1500 (m), 1397 (s), 1253 (s), 1217 (s), 1167 (w), 1084 (w), 1053 (w), 987 (w), 940 (w), 894 (m), 841 (m), 797 (s), 703 (m), 637 (w), 525 (w), 494 (w).

**Conductivity tests of ZrBPD-4F4TS and ZrBPD-4F4TS-Ox.** Sample was placed into the pipe (1.8 mm in diameter) of a glass mold, and two iron rods were inserted at both ends of the pipe (Fig. S34). The sample was pressed into a disc with a certain thickness measured by a micrometer. Two iron rods were respectively connected to the red and black probes of a multimeter. The resistance value can be recorded accurately by adjusting the appropriate ohm scale. The electronic conductivity of the sample can be calculated by the following formula:

$$\sigma = \frac{l}{R \cdot A_s}$$

where σ is the conductivity of the sample, *l* is the thickness, *R* is the resistance value and $A_s$ is the cross-sectional area. $A_s = \pi \cdot r^2$ (r is the radius of the sample piece, 0.9

mm.)

**Preparation of $H_2SO_4$@ZrBPD-4F4TS-Ox.** The solid sample of as-made ZrBPD-4F4TS-Ox (15 mg) was added into a 10 mL glass vial containing 1 M $H_2SO_4$ aqueous solution, and was then gently stirred for 1 h at room temperature. Afterwards, the resulted solid $H_2SO_4$@ZrBPD-4F4TS-Ox was isolated by centrifugation and then dried at 60 °C for 2 hours.

**Calculation for proton conductivity and activation energy.**

The Nyquist plots (Z'' *vs*. Z') of proton-conducting MOF often show a single semicircle at high frequency, representing proton resistivity contributions of bulk sample. The proton conductivity was deduced from the semicircle by fitting an equivalent circuit which consists of Rs, R1 and W1 in the frequency range from 10 MHz to 1 Hz. Rs corresponds to wire and electrode resistance, R1 is proton resistance and W1 attributes to the resistivity of grain boundary. Sometimes W1 is not necessary, because the impedance plot of the capacitive tail may not appear in the measured range due to the high magnitude of the resistivity.

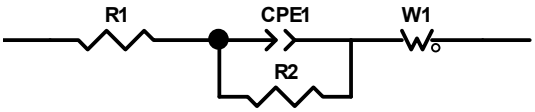


The water-assisted conductivities of synthesized materials were measured under different relative humidity and temperature conditions and were further fitted with different fitting circuits using the ZView software[5]. Proton conductivity ($\sigma$, S cm$^{-1}$) was calculated from the impedance spectra with the equation of $\sigma = l/RS$, where $l$ is the thickness (mm) and $S$ is the cross-sectional area (mm$^2$) of the pellet, while $R$ (Ω) can be calculated from the impedance plots. The activation energy values were calculated using the Arrhenius equation $\sigma T = \sigma_0 \exp(-Ea/kT)$ by the slope of the plots of ln($\sigma T$) versus 1000/$T$.

## Figures and Tables

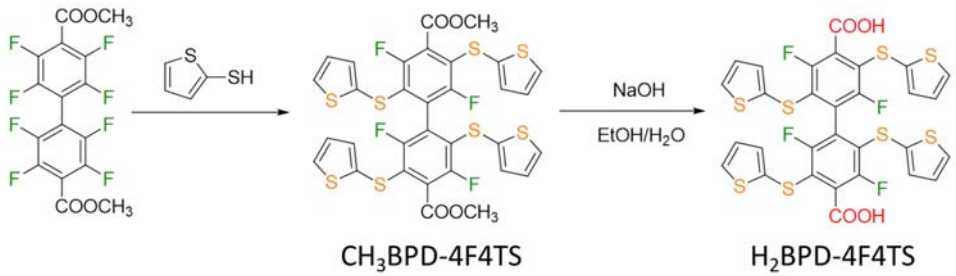


**Fig. S1** The synthetic procedure of $H_2$BPD-4F4TS.

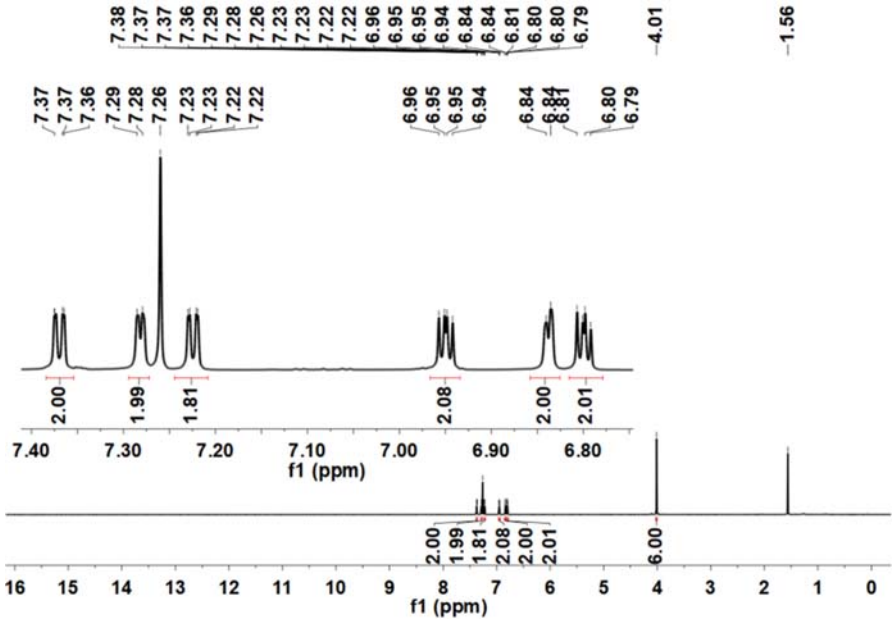


**Fig. S2** The $^1$H NMR spectrum of compound $CH_3$BPD-4F4TS in $CDCl_3$.

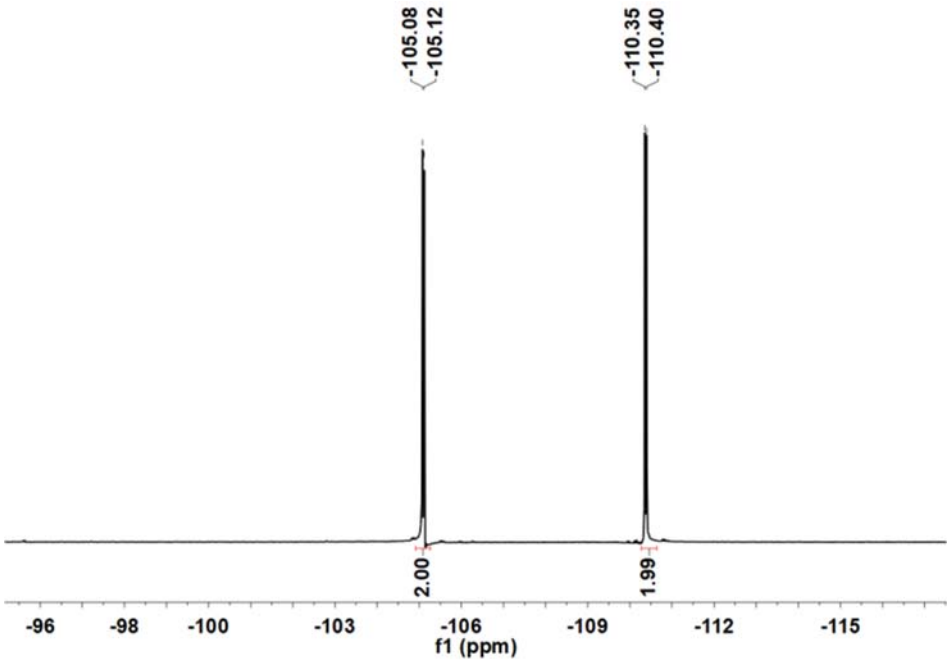


**Fig. S3** The $^{19}F$ NMR spectrum of compound $CH_3$BPD-4F4TS in $CDCl_3$.

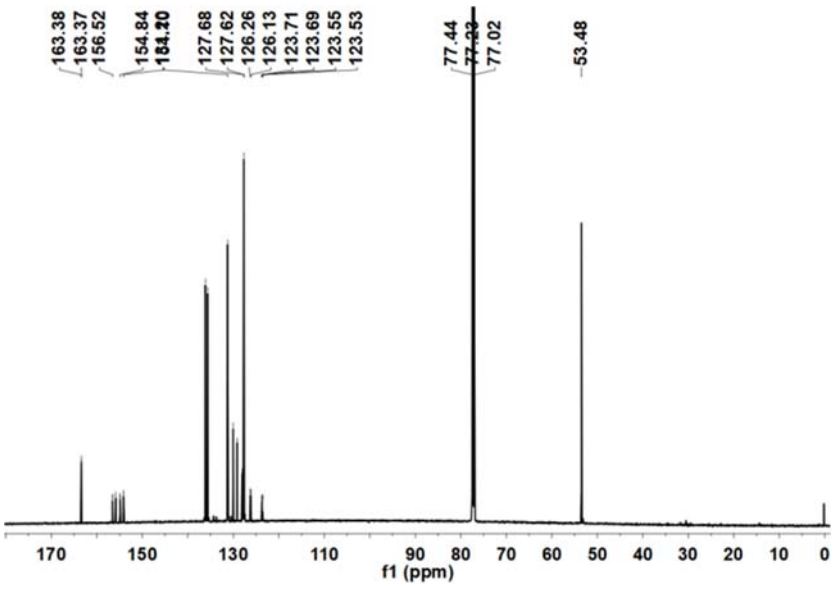


**Fig. S4** The $^{13}C$ NMR spectrum of compound $CH_3$BPD-4F4TS in $CDCl_3$.

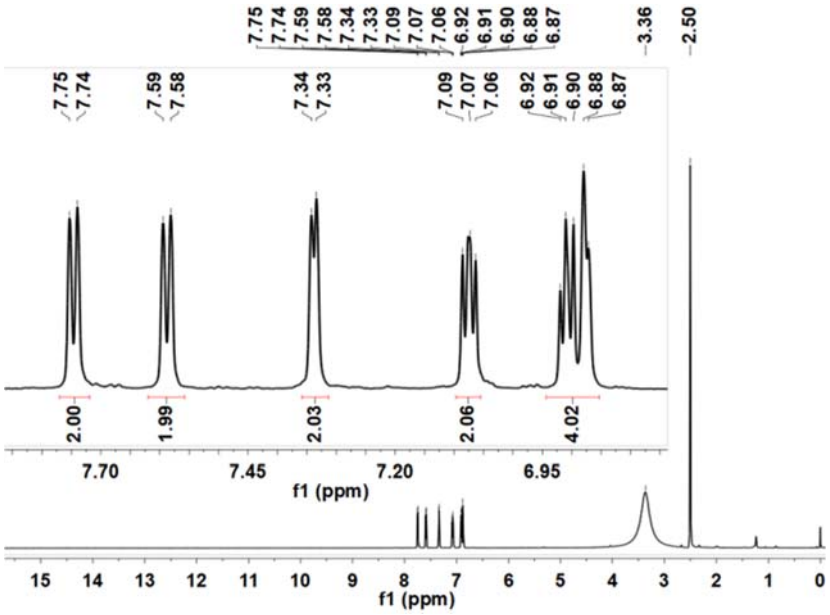


**Fig. S5** The $^{1}$H NMR spectrum of compound $H_2$BPD-4F4TS in DMSO-$d_6$.

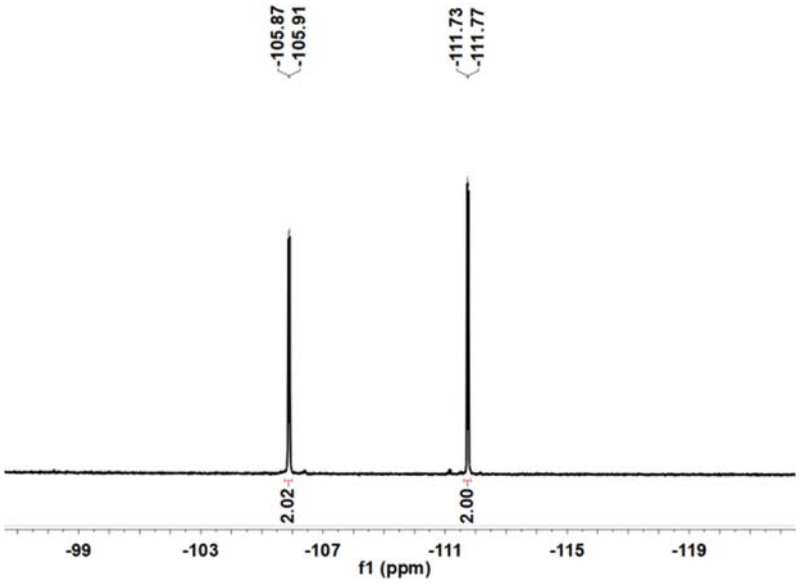


**Fig. S6** The $^{19}$F NMR spectrum of compound $H_2$BPD-4F4TS in DMSO-$d_6$.

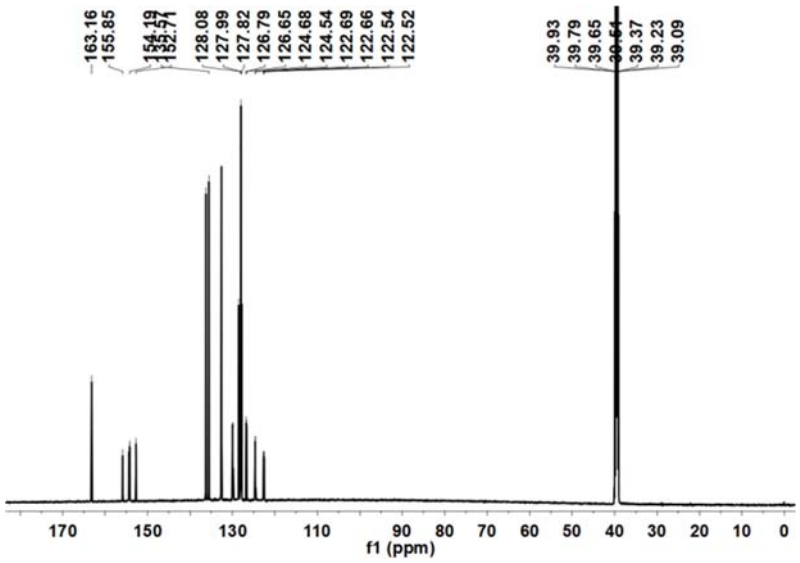


**Fig. S7** The $^{13}C$ NMR spectrum of compound $H_2$BPD-4F4TS in DMSO-$d_6$.

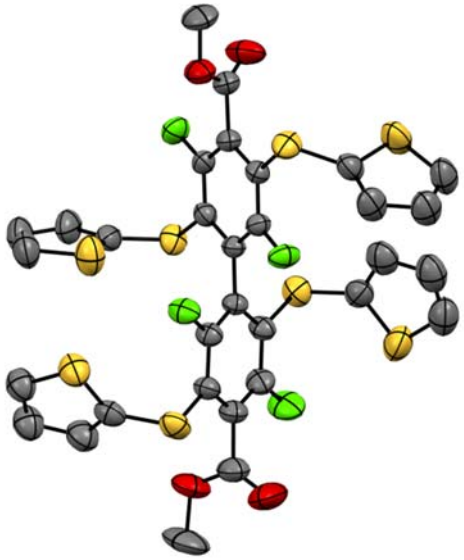

**Fig. S8** The single-crystal X-ray structure of $CH_3$BPD-4F4TS, with displacement ellipsoids at the 50% probability level. Hydrogen atoms and disorder have been omitted for clarity. Color scheme: gray, carbon; red, oxygen; orange, sulfur; green, fluorine.

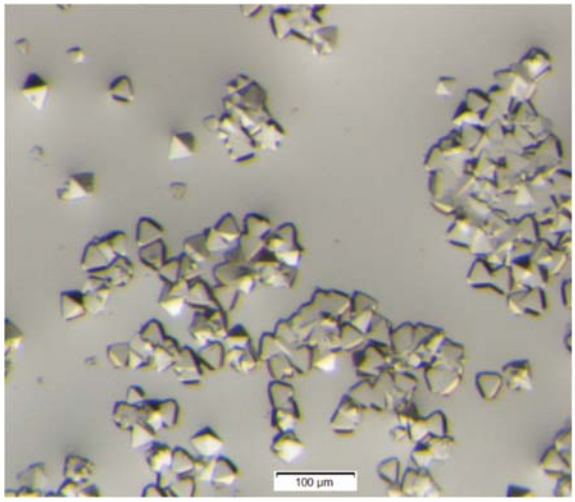


**Fig. S9** A photograph of as-made ZrBPD-4F4TS single crystals.

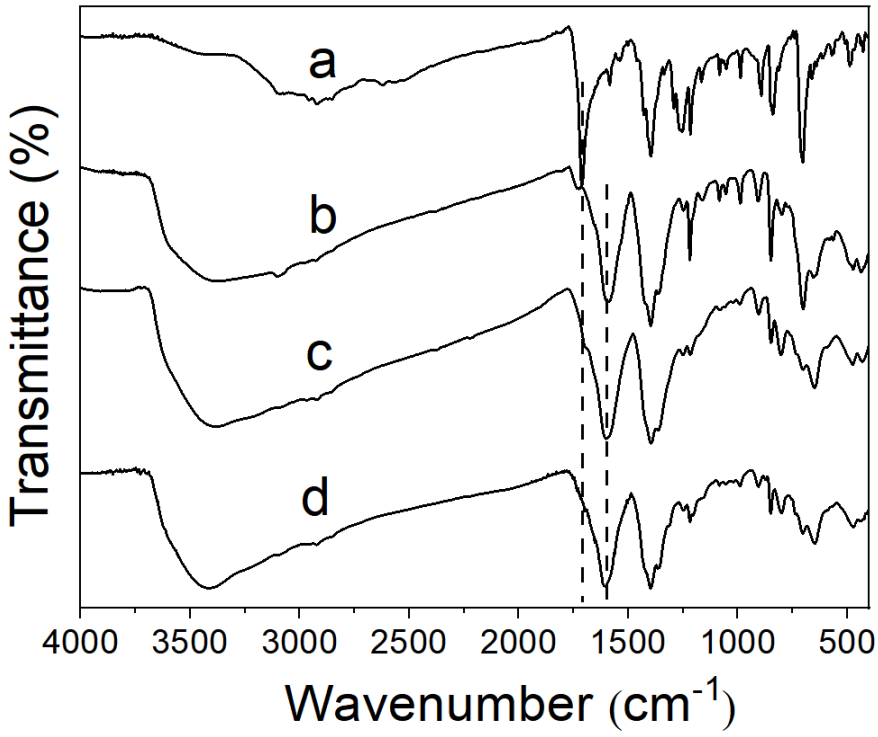


**Fig. S10** The FT-IR spectra of (a) the ligand $H_2$BPD-4F4TS, (b) as-made ZrBPD-4F4TS, (c) ZrBPD-4F4TS-Ox, (d) sample (c) after immersing in the 0.01 M NaOH (pH=12) for 30 min.

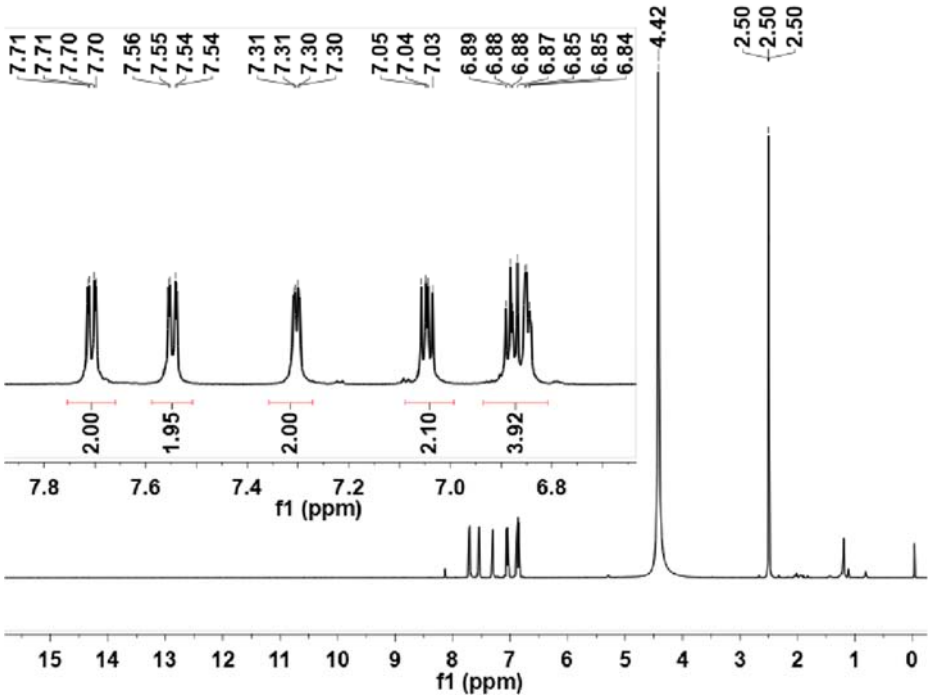


**Fig. S11** Solution $^{1}$H NMR spectra of the activated sample of ZrBPD-4F4TS ultrasonically dissolved in DCl (38 % in $D_2O$)/DMSO-$d_6$ (v:v = 1:4) solution of NaF.

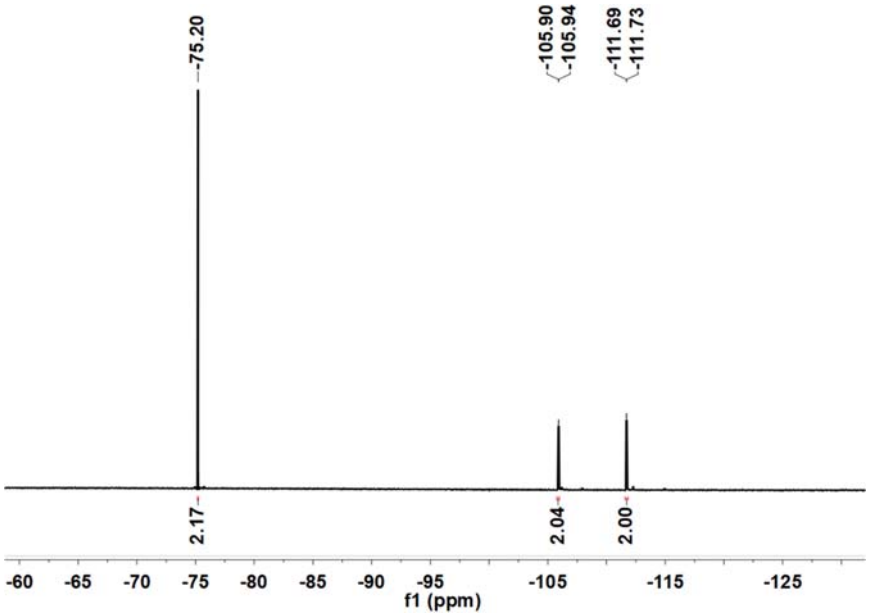


**Fig. S12** Solution $^{19}$F NMR spectra of the activated sample of ZrBPD-4F4TS ultrasonically dissolved in DCl (38 % in $D_2O$)/DMSO-$d_6$ (v:v = 1:4) solution of NaF.

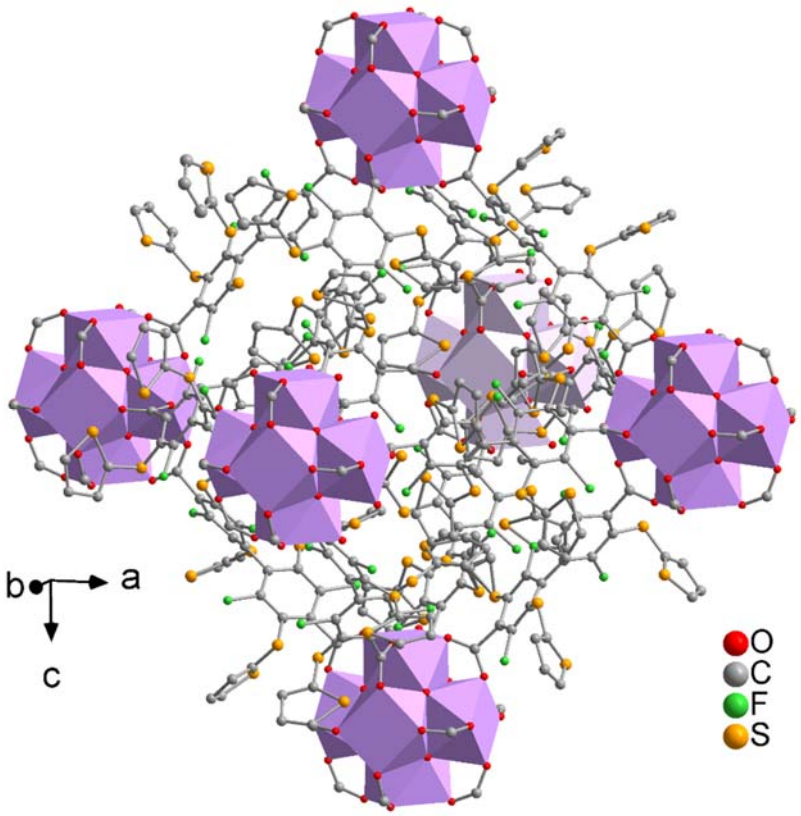


**Fig. S13** The single-crystal X-ray structure of ZrBPD-4F4TS with an octahedral unit based on Zr-O clusters. Hydrogen atoms and disorder are omitted for easy visualization. More details on crystal refinement are provided in the section of *Single crystal X-ray crystallography*.

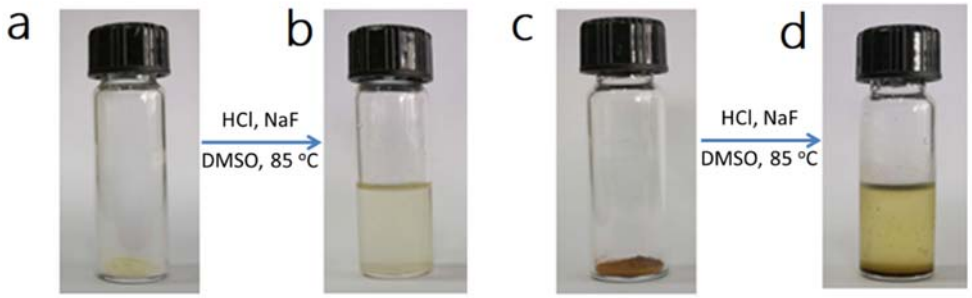


**Fig. S14** Photographs of ZrBPD-4F4TS (a, b) and ZrBPD-4F4TS-Ox (c, d) before and after treatment with 0.2% HF and 0.36% HCl solution in DMSO.

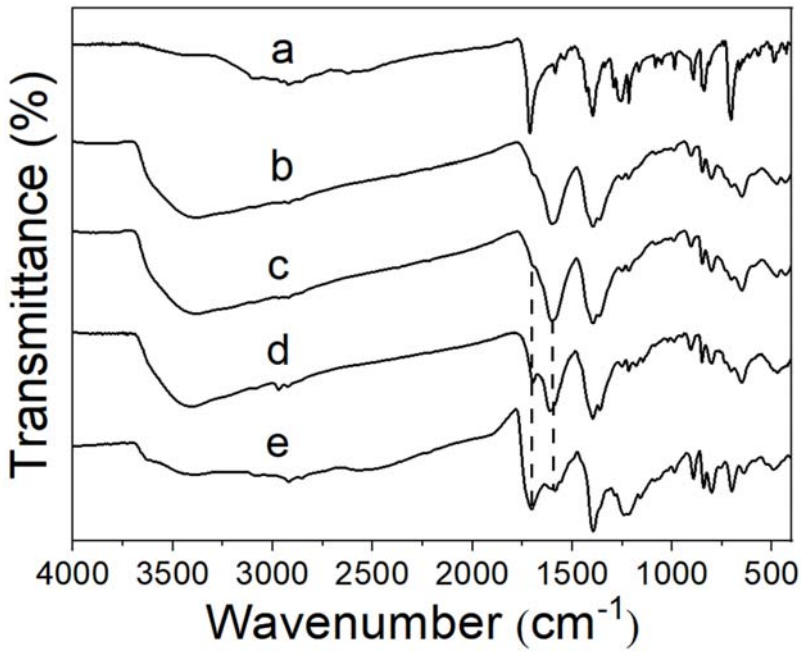


**Fig. S15** The FT-IR spectra of (a) the ligand $H_2$BPD-4F4TS, (b) as-made ZrBPD-4F4TS, (c) ZrBPD-4F4TS-Ox, (d) ZrBPD-4F4TS-Ox after treatment by a 0.2% HF/0.36% HCl DMSO solution at 85 °C, (e) ZrBPD-4F4TS-Ox after treatment by a 0.2% HF/1.8% HCl DMSO solution at 85 °C.

The ZrBPD-4F4TS-Ox sample thus treated with HF shows weakened IR feature for the asymmetric stretches of the -$CO_2^-$ group (bonded to $Zr^{4+}$) at 1607 $cm^{-1}$, and an emergent peak at 1711 $cm^{-1}$ that correspond to the stretch of free –COOH groups (spectrum d); the latter peak became more intense in higher concentration of HCl (spectrum e). The evolution of these IR features is consistent with the effective extraction of Zr(IV) by HF from the host framework of ZrBPD-4F4TS-Ox.

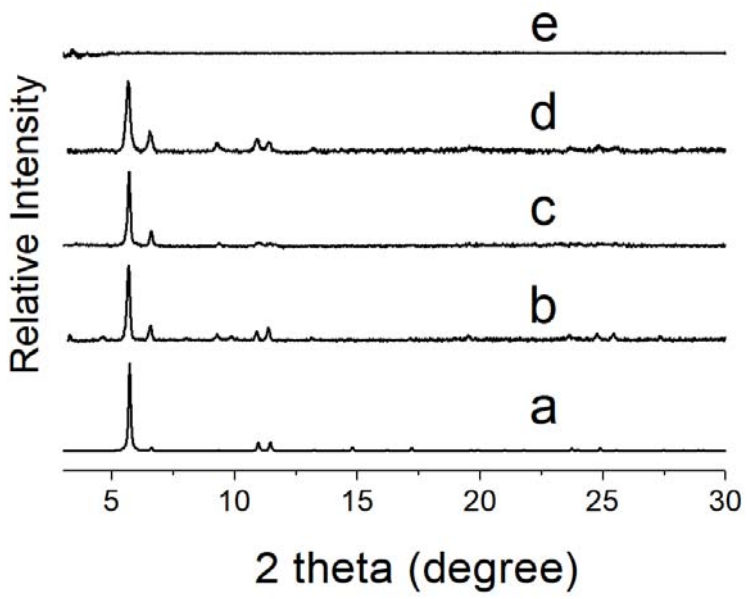


**Fig. S16** PXRD patterns of (a) simulated ZrBPD-4F4TS; (b) as-made ZrBPD-4F4TS; (c) ZrBPD-4F4TS-Ox; (d) ZrBPD-4F4TS-Ox after treatment by a 0.2% HF/0.36% HCl DMSO solution at 85 °C; (e) ZrBPD-4F4TS-Ox after treatment by a 0.2% HF/1.8% HCl DMSO solution at 85 °C.

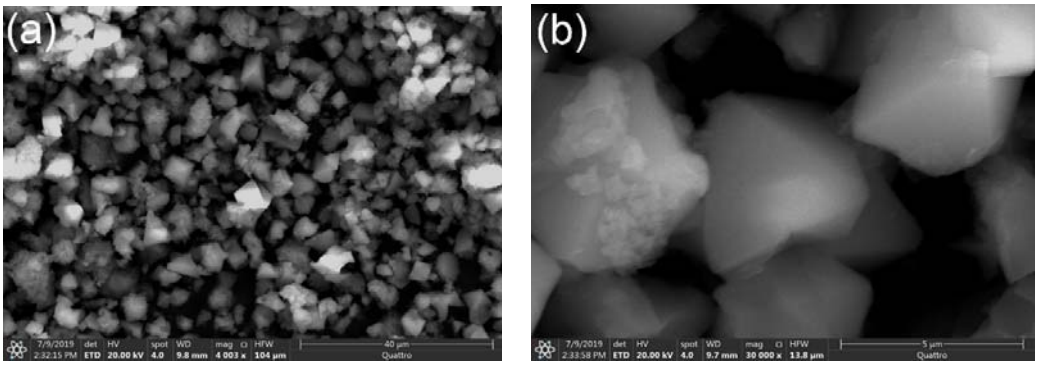


**Fig. S17** SEM images of ZrBPD-4F4TS-Ox after treatment by a 0.2% HF/0.36% HCl DMSO solution at 85 °C.

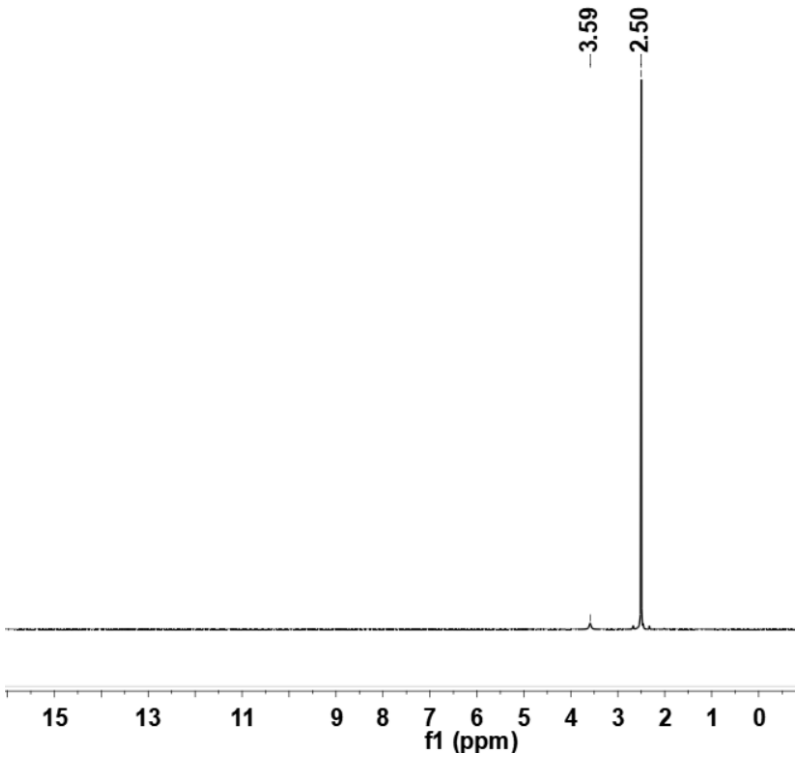


**Fig. S18** Solution $^{1}H$ NMR spectrum of ZrBPD-4F4TS-Ox after treatment by a 0.2% HF/1.8% HCl DMSO solution at 85 °C.

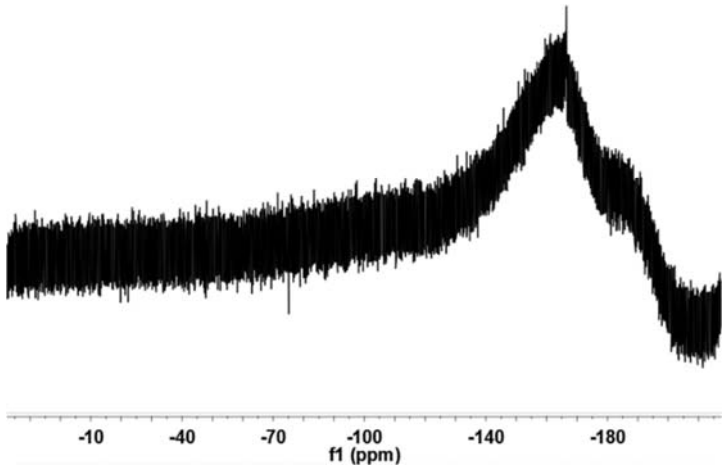


**Fig. S19** Solution $^{19}F$ NMR spectrum of ZrBPD-4F4TS-Ox after treatment by a 0.2% HF/1.8% HCl DMSO solution at 85 °C.

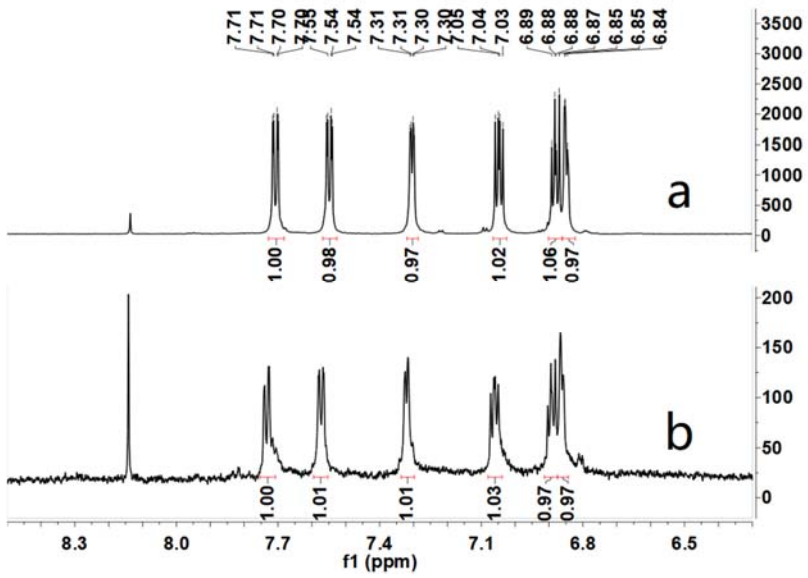


**Fig. S20** Solution $^{1}$H NMR spectrum of (a) activated sample of ZrBPD-4F4TS ultrasonically dissolved in DCl (38 % in $D_2O$)/DMSO-$d_6$ (v:v = 1:4) solution of NaF; (b) ZrBPD-4F4TS oxidized by less $FeCl_3$ (0.5:1 $FeCl_3$/thiophene) after treatment by a 0.2% HF/0.36% HCl DMSO solution at 85 °C.

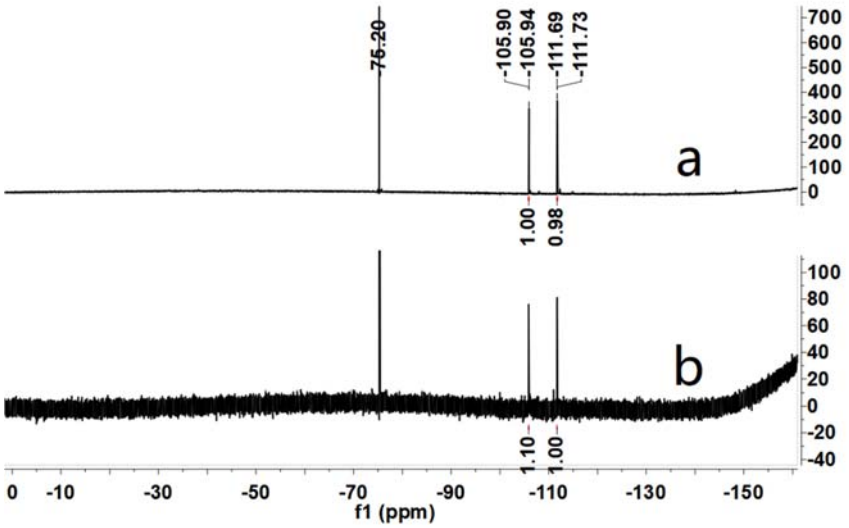


**Fig. S21** Solution $^{19}$F NMR spectrum of (a) activated sample of ZrBPD-4F4TS ultrasonically dissolved in DCl (38 % in $D_2O$)/DMSO-$d_6$ (v:v = 1:4) solution of NaF; (b) ZrBPD-4F4TS oxidized by less $FeCl_3$ (0.5:1 $FeCl_3$/thiophene) after treatment by a 0.2% HF/0.36% HCl DMSO solution at 85 °C.

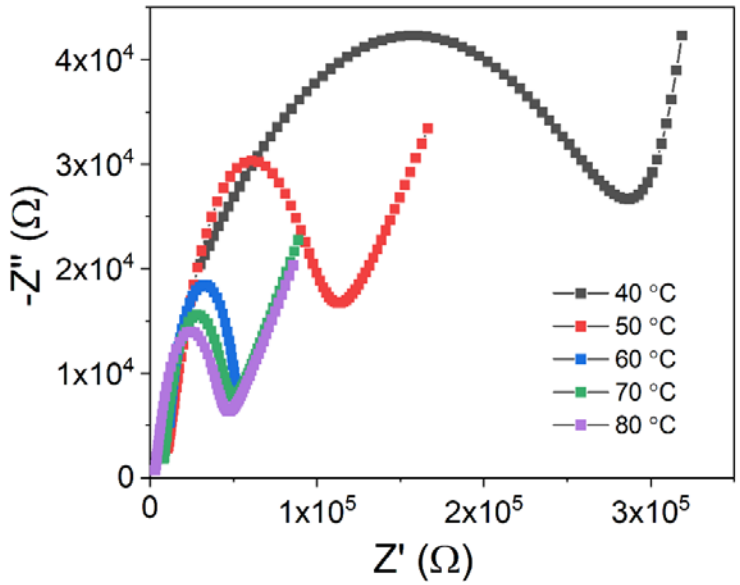


**Fig. S22** Nyquist plots of ZrBPD-4F4TS at different temperatures (from 40 °C to 80 °C) and 90% RH.

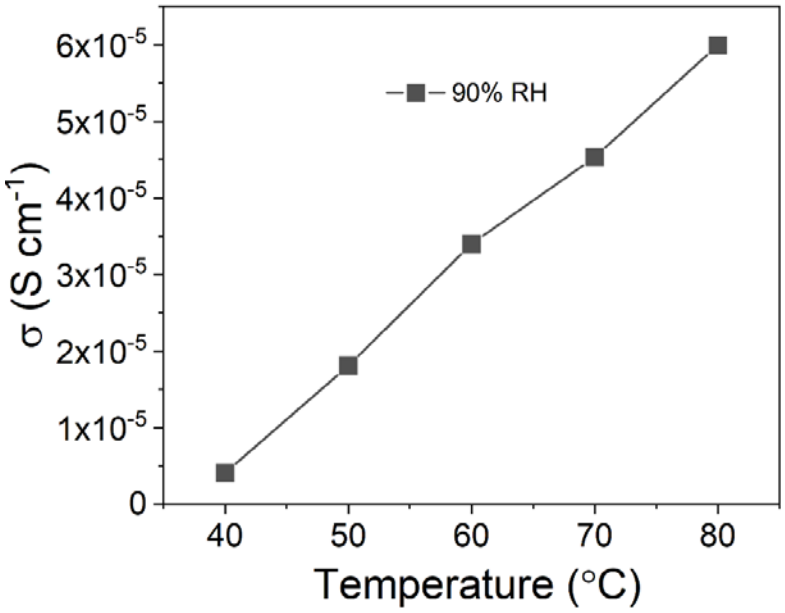


**Fig. S23** Proton conductivity of ZrBPD-4F4TS at different temperatures (from 40 °C to 80 °C) and 90% RH.

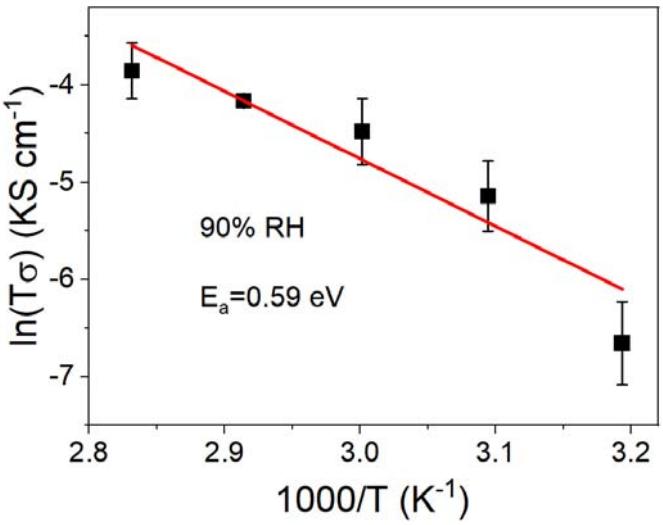


**Fig. S24** Arrhenius plot of conductivities for bulk contribution to resistivity of ZrBPD-4F4TS at 90% RH.

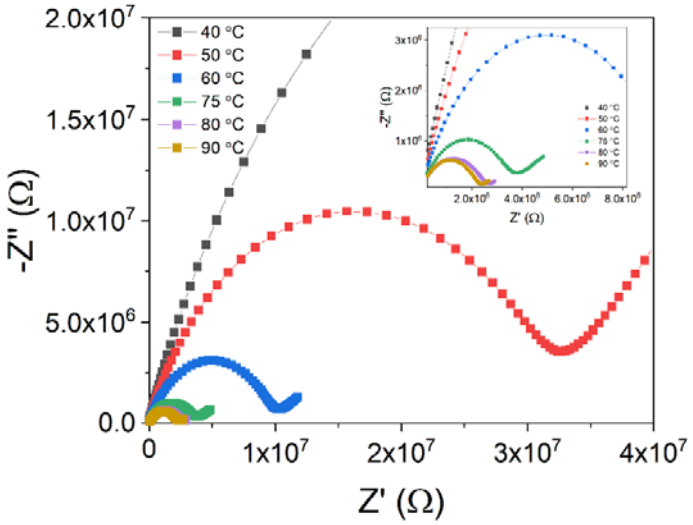


**Fig. S25** Nyquist plots of ZrBPD-4F4TS-Ox at different temperatures (from 40 °C to 90 °C) and 90% RH.

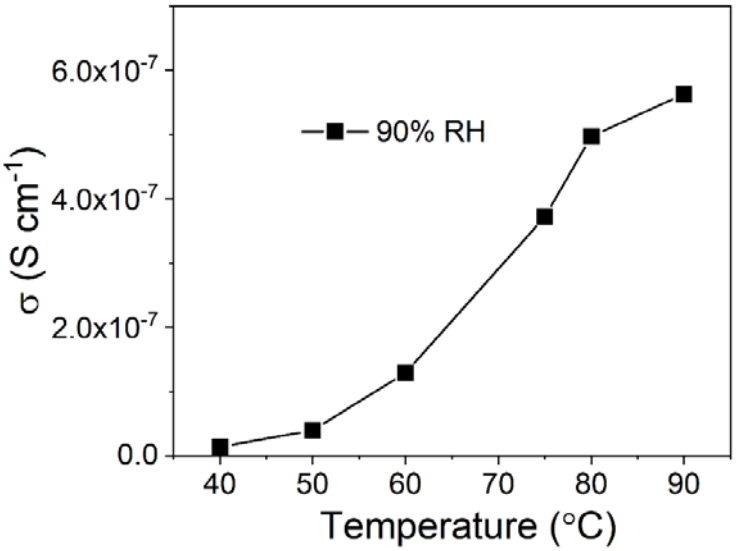


**Fig. S26** Proton conductivity of ZrBPD-4F4TS-Ox at different temperatures (from 40 °C to 90 °C) and 90% RH.

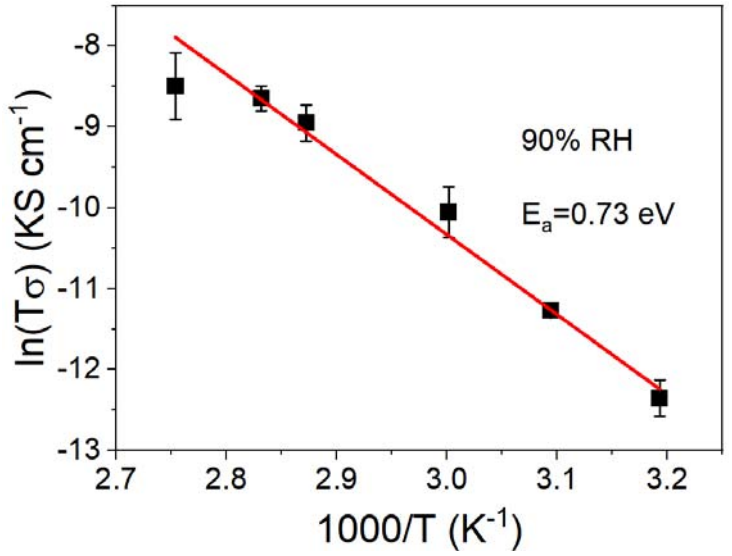


**Fig. S27** An Arrhenius plot of conductivities for bulk contribution to resistivity of ZrBPD-4F4TS-Ox at 90% RH.

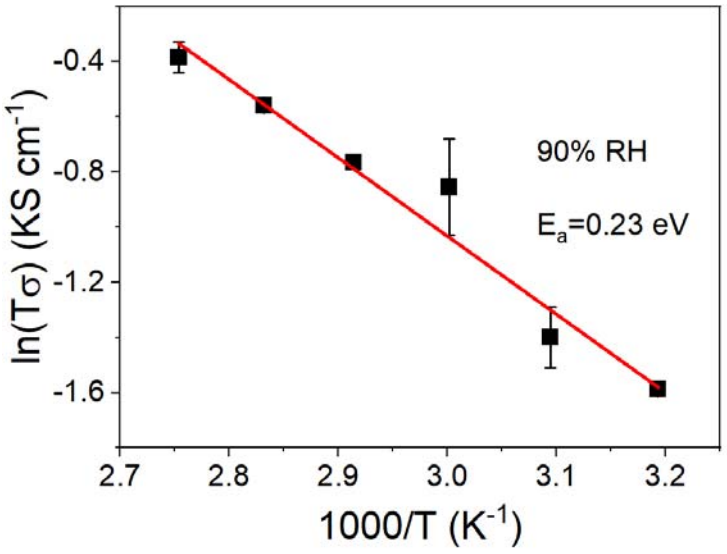


**Fig. S28** An Arrhenius plot of conductivities for bulk contribution to resistivity of $H_2SO_4$@ZrBPD-4F4TS-Ox at 90% RH.

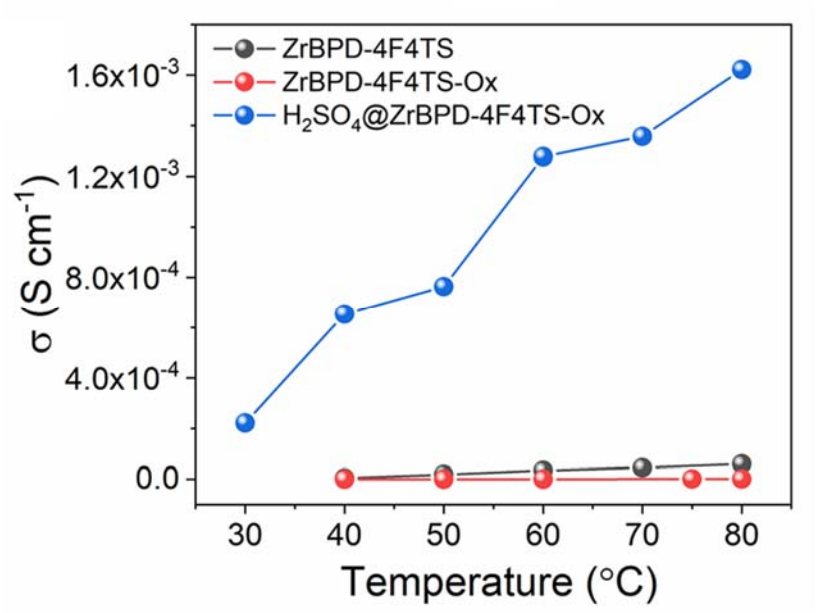


**Fig. S29** Proton conductivities of ZrBPD-4F4TS, ZrBPD-4F4TS-Ox, and $H_2SO_4$@ZrBPD-4F4TS-Ox at different temperatures and 90% RH.

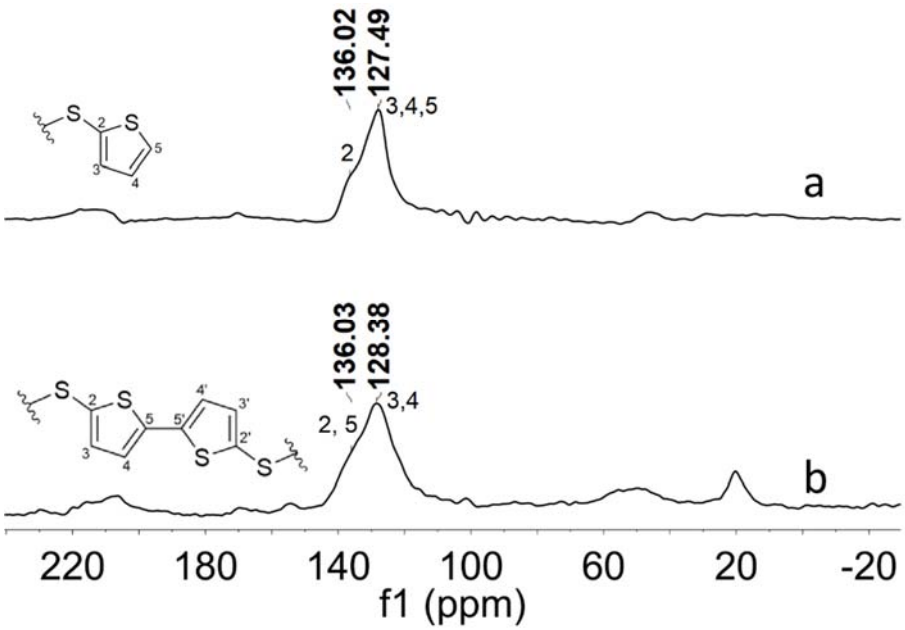


**Fig. S30** The solid state $^{13}C$ NMR of activated samples of (a) ZrBPD-4F4TS and (b) ZrBPD-4F4TS-Ox.

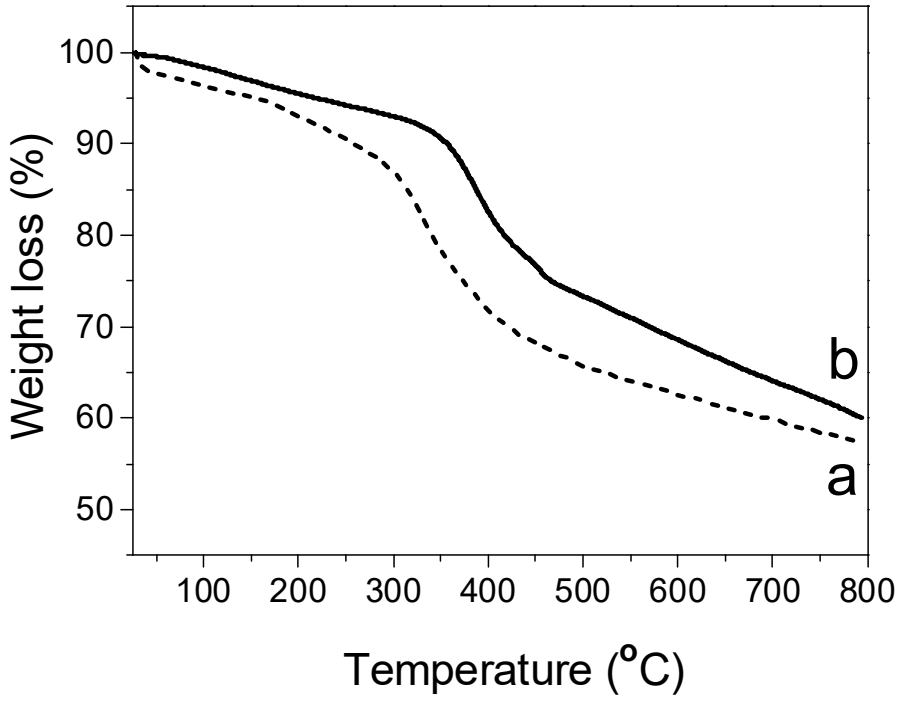


**Fig. S31** The thermogravimetric analysis (TGA) plots of as-made sample of (a, dash) ZrBPD-4F4TS and (b, solid) ZrBPD-4F4TS-Ox.

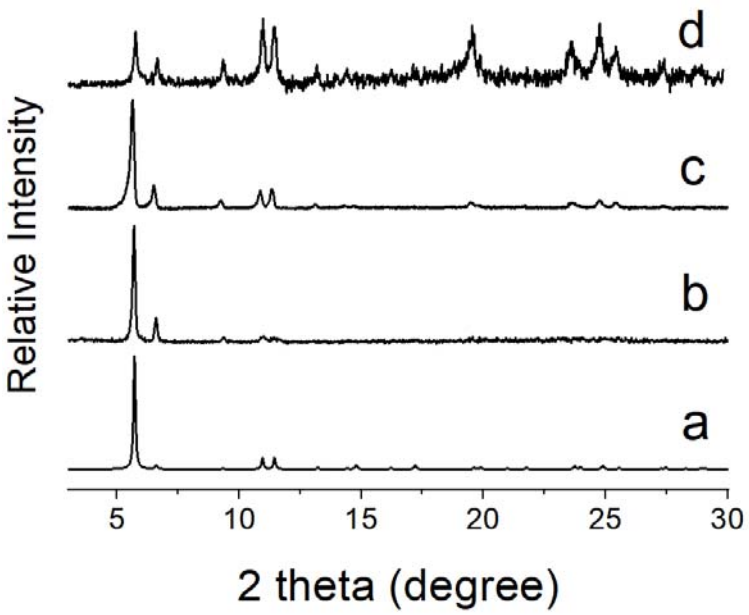


**Fig. S32** PXRD patterns of (a) simulated ZrBPD-4F4TS, (b) as-made ZrBPD-4F4TS, (c) activated ZrBPD-4F4TS and (d) ZrBPD-4F4TS after $N_2$ and $CO_2$ gas sorption tests.

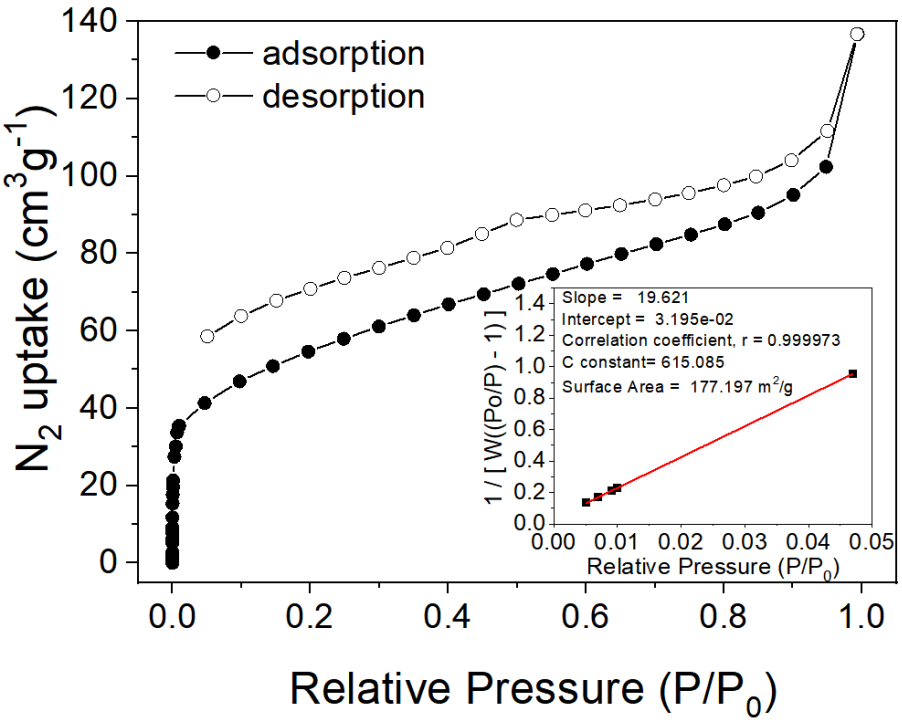


**Fig. S33** $N_2$ adsorption and desorption isotherms for activated ZrBPD-4F4TS at 77 K.

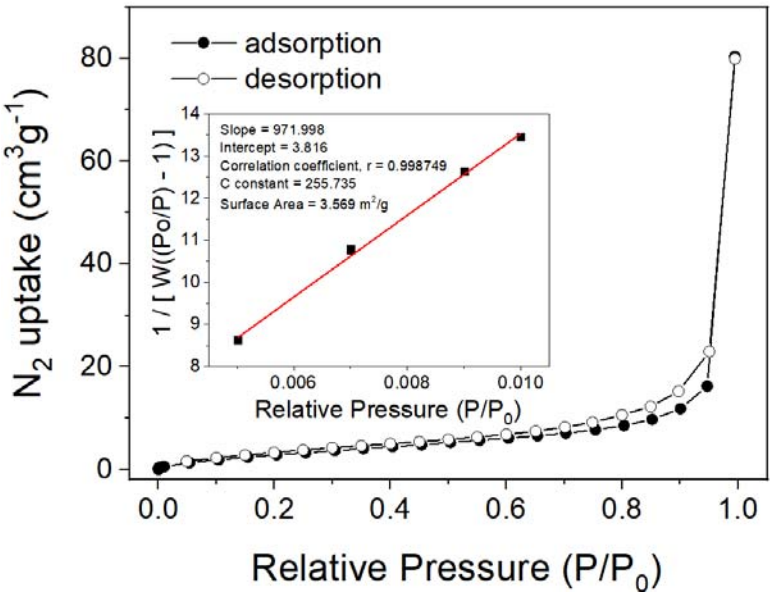


**Fig. S34** $N_2$ adsorption and desorption isotherms for activated ZrBPD-4F4TS-Ox at 77 K.

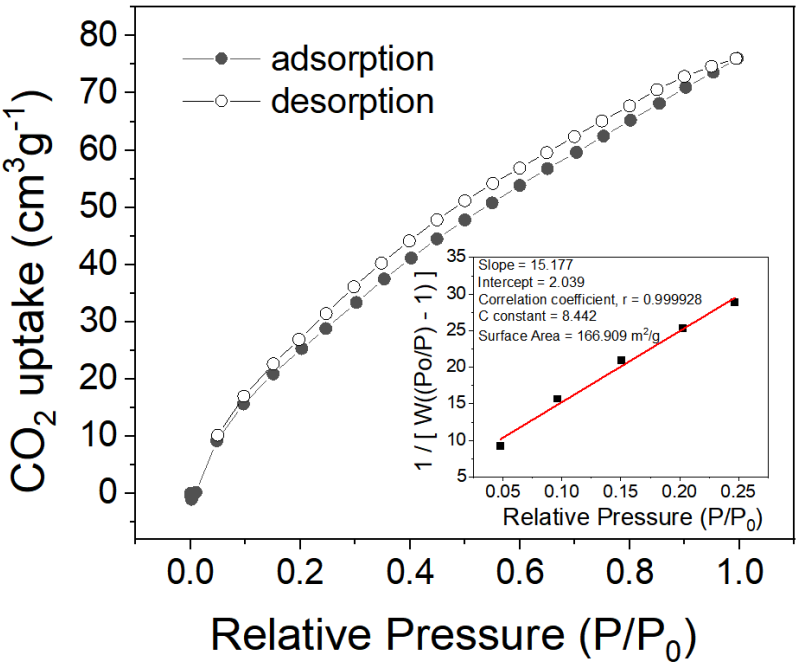


**Fig. S35** $CO_2$ adsorption and desorption isotherms for activated ZrBPD-4F4TS at 195 K.

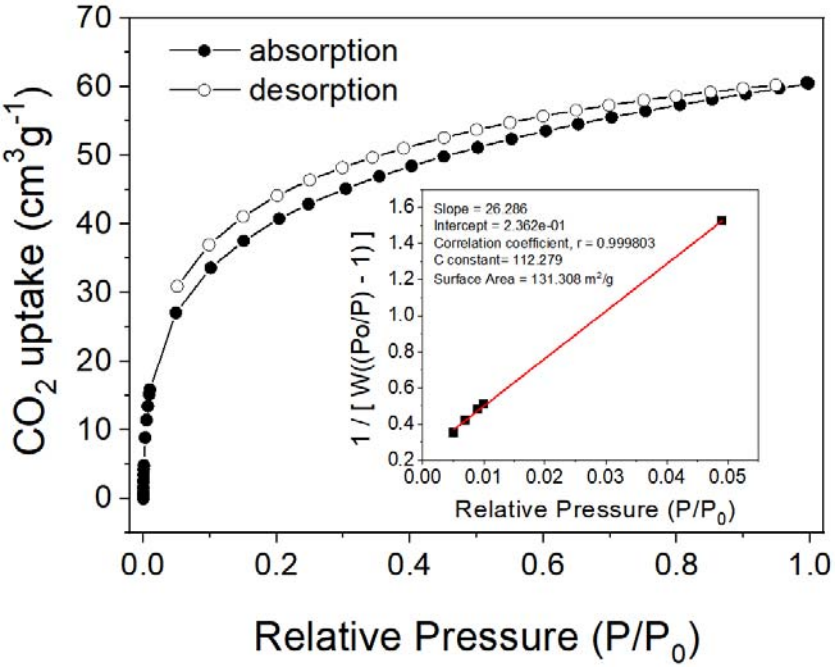


**Fig. S36** $CO_2$ adsorption and desorption isotherms for activated ZrBPD-4F4TS-Ox at 195 K.

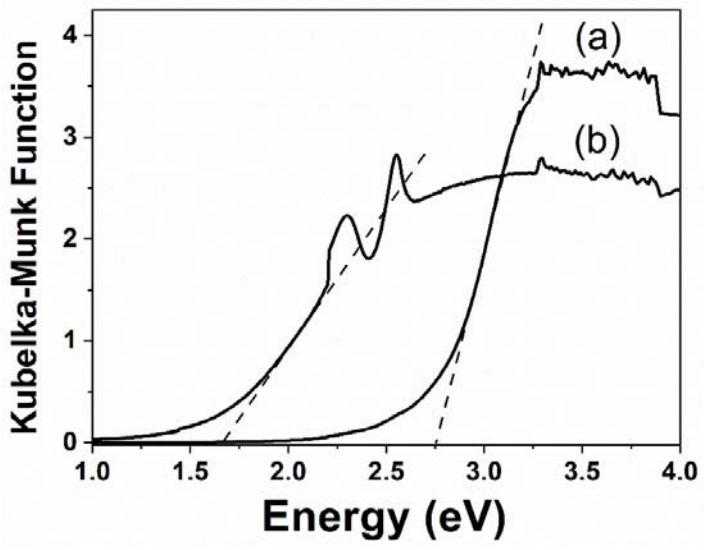


**Fig. S37** Diffuse reflectance spectra for activated (a) ZrBPD-4F4TS and (b) ZrBPD-4F4TS-Ox.

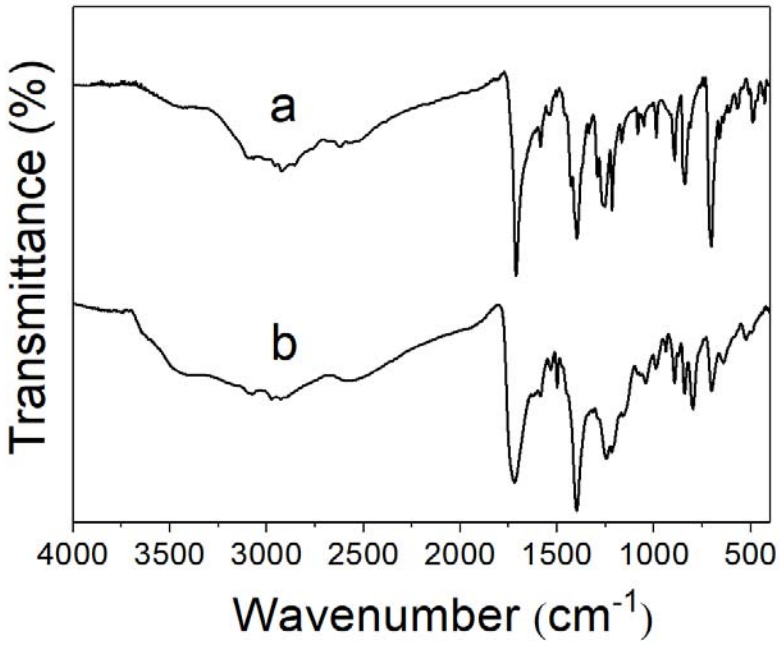


**Fig. S38** The FT-IR spectra of (a) the ligand $H_2$BPD-4F4TS; and (b) the solution polymerized product $H_2$BPD-4F4TS-*p*.

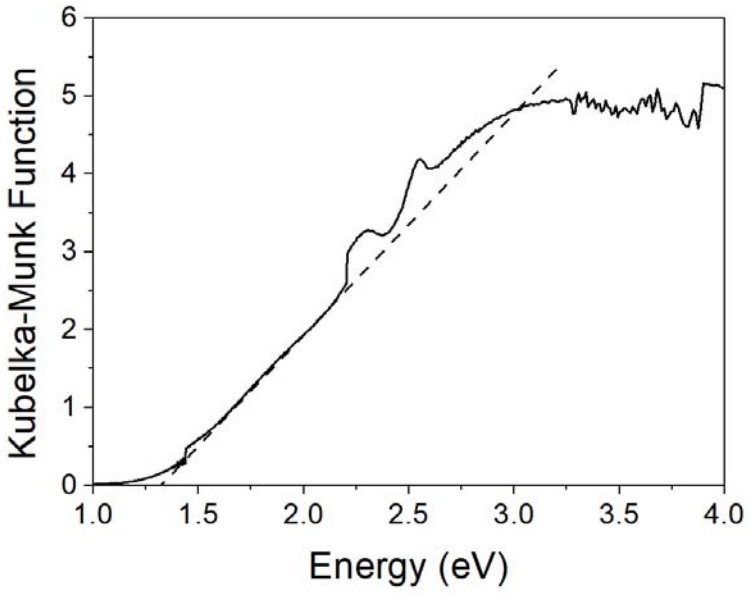


**Fig. S39** The diffuse reflectance spectrum for solution polymerized product of $H_2$BPD-4F4TS-*p*, which compares well with that of ZrBPD-4F4TS-Ox (Fig. S37, spectrum b).


**Fig. S40** A photograph of the setup for electronic conductivity measurement.

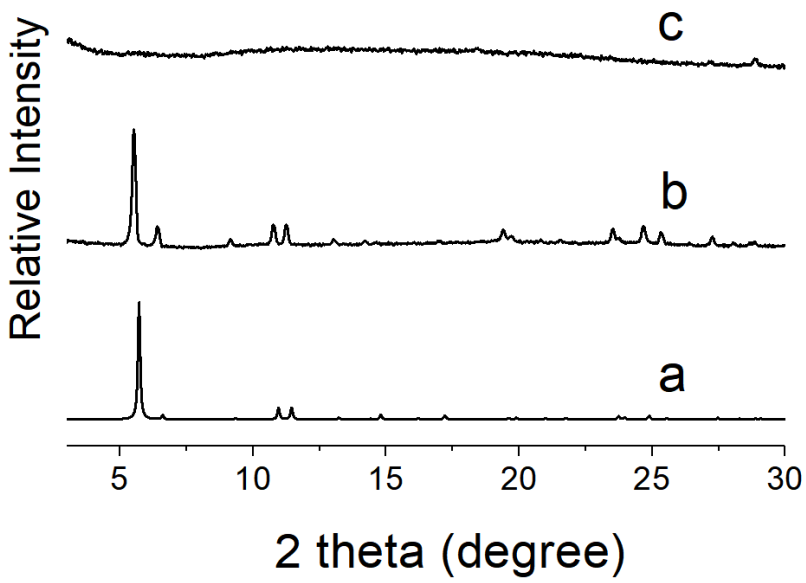


**Fig. S41** PXRD patterns of (a) simulated ZrBPD-4F4TS; (b) ZrBPD-4F4TS oxidized by less $FeCl_3$ (0.5:1 $FeCl_3$/thiophene); (c) sample (b) after treatment by a 0.2% HF/0.36% HCl DMSO solution at 85 °C.

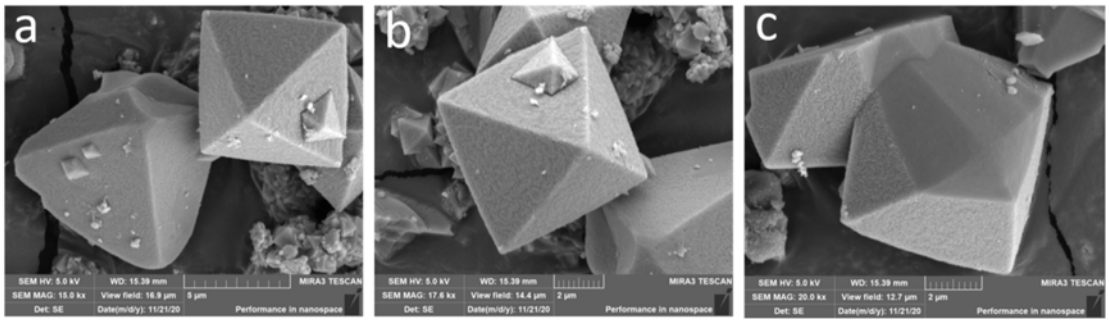


**Fig. S42** SEM images (a-c) of ZrBPD-4F4TS-Ox after treatment by a 0.2% HF/0.36% HCl DMSO solution at 85 °C (Images retaken for compositional comparison between the big crystals and the smaller particles).

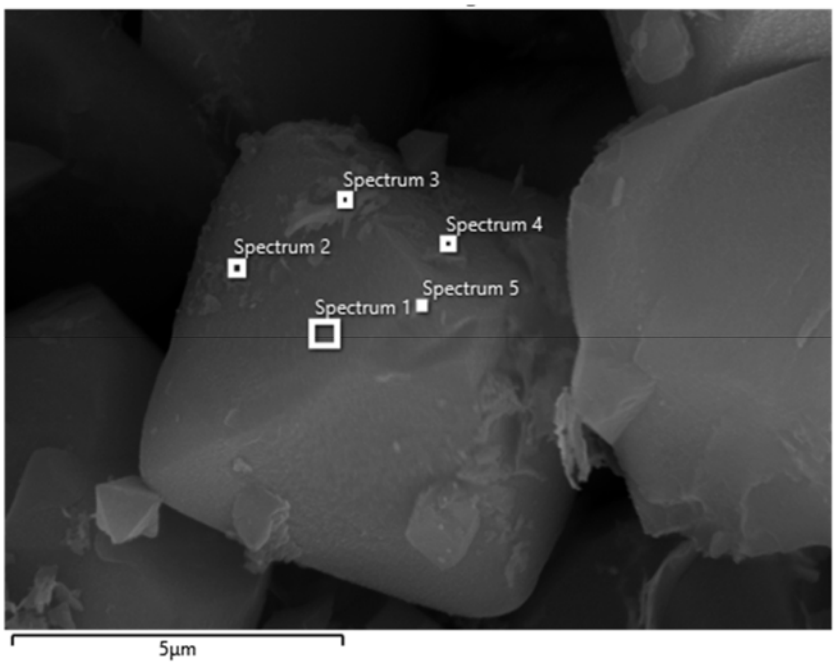


**Fig. S43** SEM image of ZrBPD-4F4TS-Ox after treatment by a 0.2% HF/0.36% HCl DMSO solution at 85 °C, with marked small particles for local elemental profiling (see following five spectra below for the results).

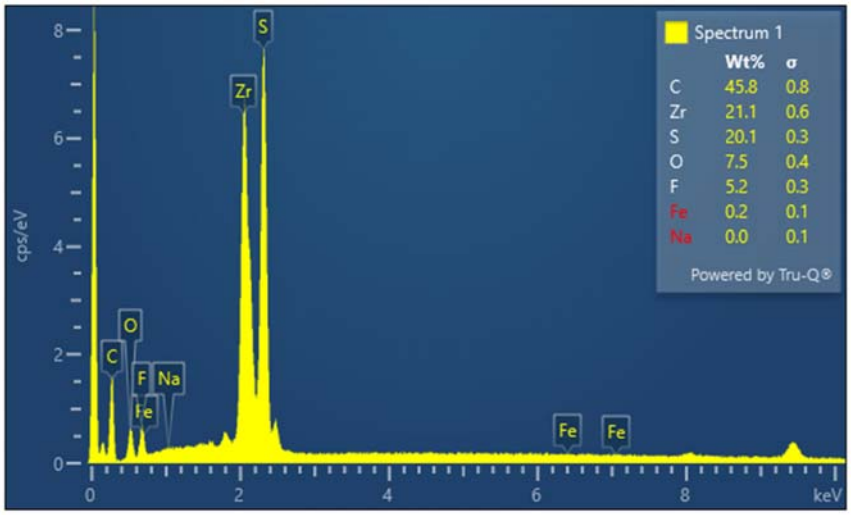


**Fig. S44** A selected area (spectrum 1 of Fig. S41) EDS elemental analysis results of ZrBPD-4F4TS-Ox after treatment by a 0.2% HF/0.36% HCl DMSO solution at 85 °C.

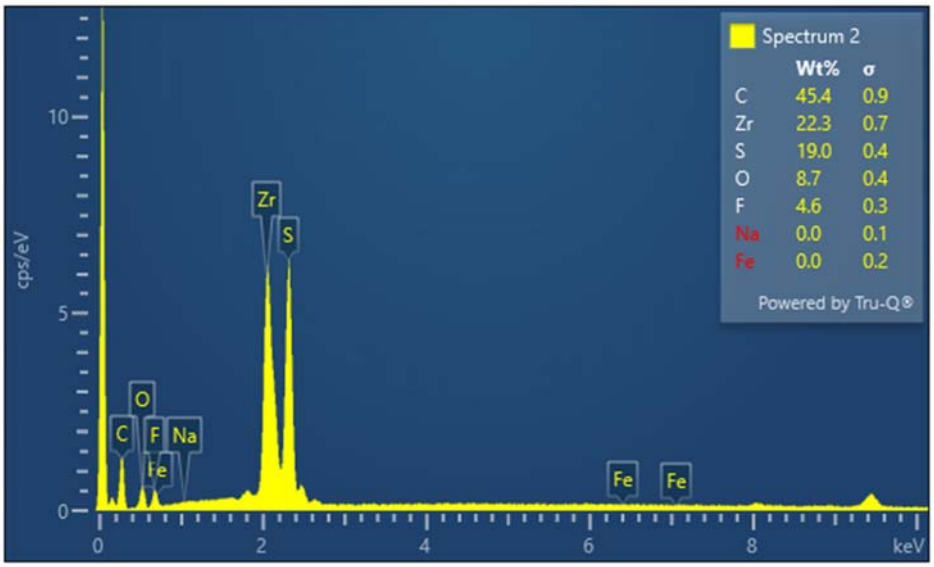


**Fig. S45** A selected area (spectrum 2 of Fig. S41) EDS elemental analysis results of ZrBPD-4F4TS-Ox after treatment by a 0.2% HF/0.36% HCl DMSO solution at 85 °C.

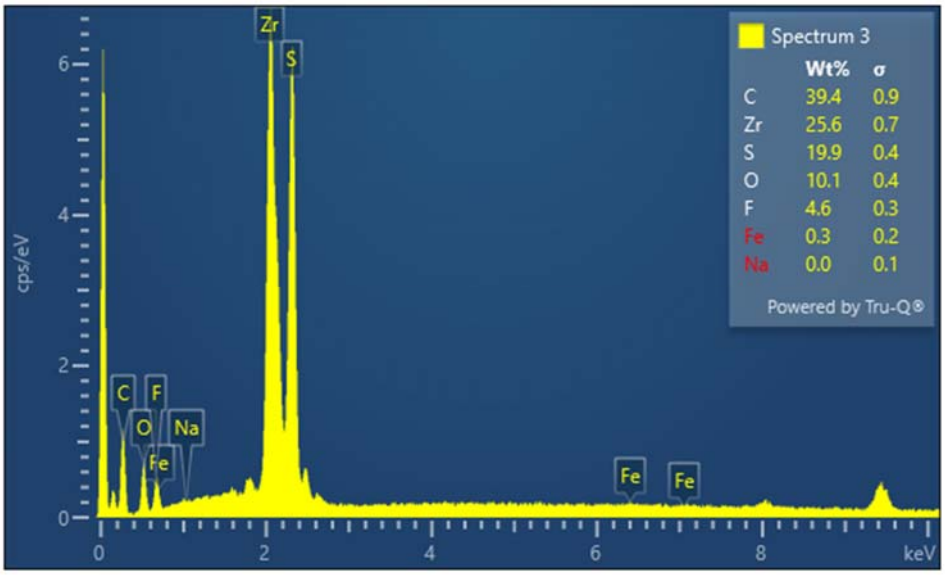


**Fig. S46** A selected area (spectrum 3 of Fig. S41) EDS elemental analysis results of ZrBPD-4F4TS-Ox after treatment by a 0.2% HF/0.36% HCl DMSO solution at 85 °C.

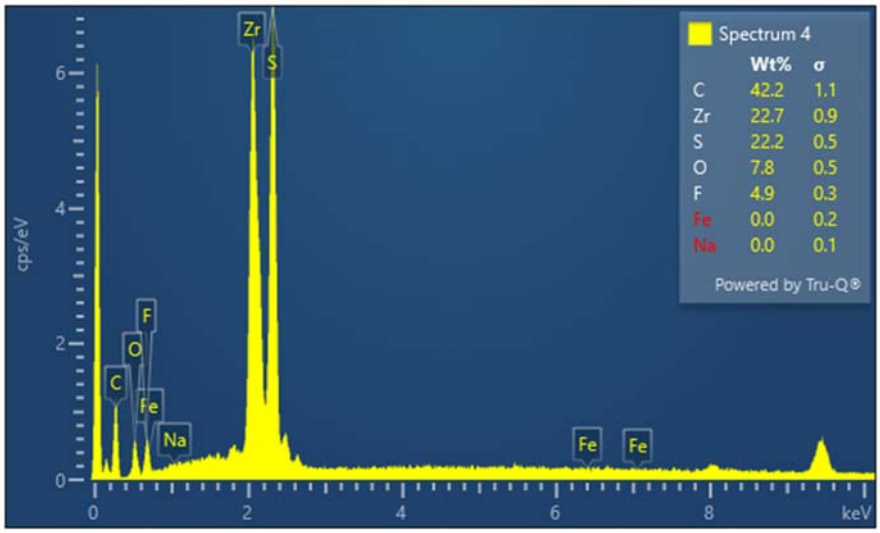


**Fig. S47** A selected area (spectrum 4 of Fig. S41) EDS elemental analysis results of ZrBPD-4F4TS-Ox after treatment by a 0.2% HF/0.36% HCl DMSO solution at 85 °C.

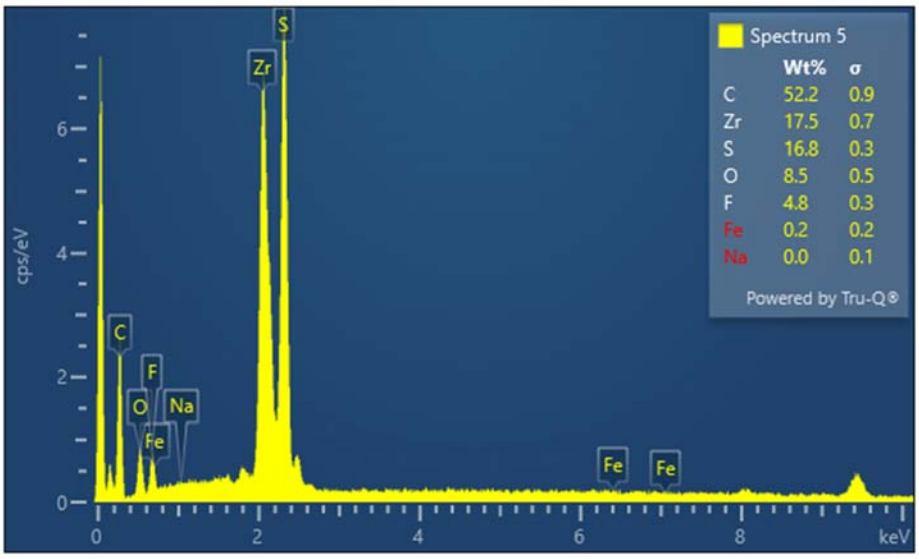


**Fig. S48** A selected area (spectrum 5 of Fig. S41) EDS elemental analysis results of ZrBPD-4F4TS-Ox after treatment by a 0.2% HF/0.36% HCl DMSO solution at 85 °C.

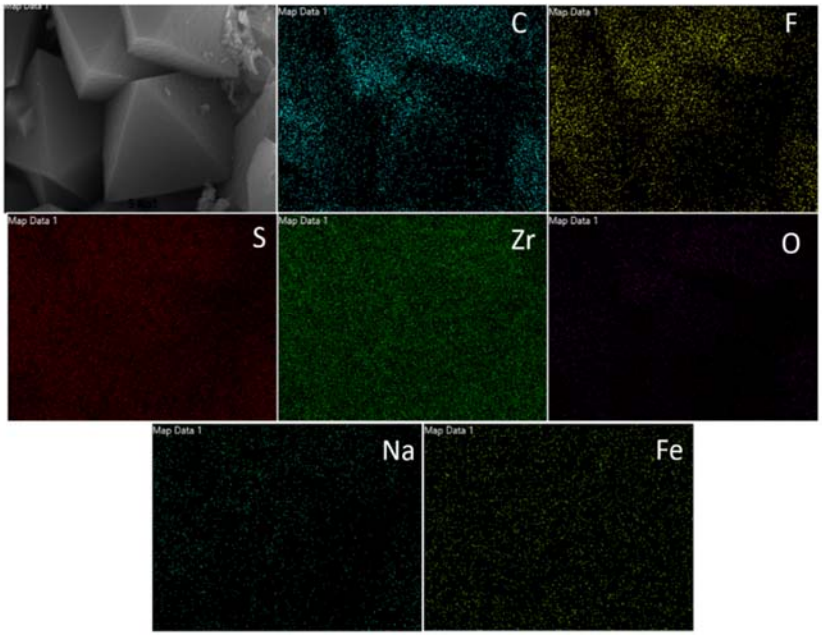


**Fig. S49** An elemental mapping (showing the uniform distribution of elements) of ZrBPD-4F4TS-Ox after treatment by a 0.2% HF/0.36% HCl DMSO solution at 85 °C.

**Table S1** Crystallographic refinement parameters and results of $CH_3$BPD-4F4TS.

| Compound | $CH_3$BPD-4F4TS |
|---|---|
| Empirical formula | $C_{32}H_{18}F_4O_4S_8$ |
| Formula weight | 798.94 |
| Temperature/K | 300.0 |
| Crystal system | monoclinic |
| Space group | $P2_1/c$ |
| *a*/Å | 18.134(2) |
| *b*/Å | 10.7534(12) |
| *c*/Å | 20.059(2) |
| *α*/° | 90.00 |
| *β*/° | 117.509(7) |
| *γ*/° | 90.00 |
| Volume/Å$^3$ | 3469.3(7) |
| Z | 4 |
| Dc/g·cm$^{-3}$ | 1.530 |
| μ/mm$^{-1}$ | 5.287 |
| F(000) | 1624.0 |
| $wR_2$[b](all data) | 0.1616 |
| $R_1$[a](I>=2σ (I)) | 0.0528 |
| GOOF | 1.046 |

[a] $R_1=\sum(||F_0|-|F_c||)/\sum|F_0|$; [b] $wR_2=(\sum w(F_0^2-F_c^2)^2/\sum w(F_0^2)^2)^{1/2}$

**Table S2** Parameters and results of electronic conductivity measurement for ZrBPD-4F4TS and ZrBPD-4F4TS-Ox.

| | ZrBPD-4F4TS | ZrBPD-4F4TS-Ox |
|---|---|---|
| R (kΩ) | 181 | 1.07 |
| l (mm) | 0.51 | 0.59 |
| r (mm) | 0.9 | 0.9 |
| σ (S·cm$^{-1}$) | 1.1×10$^{-5}$ | 2.2×10$^{-3}$ |

**Table S3** Proton conductivity of ZrBPD-4F4TS, ZrBPD-4F4TS-Ox and $H_2SO_4$@ZrBPD-4F4TS-Ox at different temperatures and 90% RH.

| Temperature / σ / Sample (S cm$^{-1}$) | 40 °C | 50 °C | 60 °C | 70 °C | 75 °C | 80 °C | 90 °C |
|---|---|---|---|---|---|---|---|
| ZrBPD-4F4TS | 4.11×10$^{-6}$ | 1.81×10$^{-5}$ | 3.40×10$^{-5}$ | 4.53×10$^{-5}$ | -- | 5.99×10$^{-5}$ | -- |
| ZrBPD-4F4TS-Ox | 1.38×10$^{-8}$ | 3.96×10$^{-8}$ | 1.29×10$^{-7}$ | -- | 3.72×10$^{-7}$ | 4.97×10$^{-7}$ | 5.63×10$^{-7}$ |
| $H_2SO_4$@ZrBPD-4F4TS-Ox | 6.53×10$^{-4}$ | 7.63×10$^{-4}$ | 1.28×10$^{-3}$ | 1.36×10$^{-3}$ | -- | 1.62×10$^{-3}$ | 1.87×10$^{-3}$ |

## References:

(1) G. Sheldrick, *Acta Crystallogr A*, 2008, **64**, 112.

(2) G. Sheldrick, *Acta Crystallogr C*, 2015, **71**, 3.

(3) C. B. Hubschle, G. M. Sheldrick and B. Dittrich, *J. Appl. Crystallogr.*, 2011, **44**, 1281.

(4) L. Kissel and R. H. Pratt, *Acta Crystallogr A*, 1990, **46**, 170.

(5) D. Vladikova, P. Zoltowski, E. Makowska and Z. Stoynov, *Electrochim. Acta*, 2002, **47**, 2943.